Satellite-Derived Surface Radiation Budget over the African Continent. Part I: Estimation of Downward Solar Irradiance and Albedo

MAMOUDOU B. BA*

Department of Meteorology, The Florida State University, Tallahassee, Florida

ROBERT FROUIN

Scripps Institution of Oceanography, University of California, San Diego, La Jolla, California

SHARON E. NICHOLSON

Department of Meteorology, The Florida State University, Tallahassee, Florida

GÉRARD DEDIEU

CESBIO/LERTS, Toulouse, France

(Manuscript received 27 May 1999, in final form 9 March 2000)

ABSTRACT

Downward surface solar irradiance and albedo of the African continent are estimated from Meteosat B2 data at 30-km spatial resolution. The algorithm, based on Dedieu et al.'s approach, is verified against other satellite estimates and ground-based measurements. In the computations, the International Satellite Cloud Climatology Project's (ISCCP) radiometric calibration is adjusted using the Libyan desert as a reference target of constant reflectance properties. Surface albedo is corrected for sun zenith angle effects, allowing for better detection of seasonal changes due to the vegetation cycle. The estimates obtained with Meteosat B2 data agree generally well with other satellite estimates, although biases of 20 W m^{-2} (downward surface solar irradiance) and 0.15 (surface albedo) are obtained in some cases. There is evidence, from comparisons with surface measurements, that the clear-sky downward surface solar irradiance is overestimated over semiarid regions of Africa because of uncertainties in aerosol characteristics. In the Sahel region, where spatial albedo gradients are high, it is advantageous to use 30-km Meteosat B2 products instead of the current, coarser 280-km-resolution ISCCP products.

1. Introduction

Better scientific understanding and prediction of climate fluctuations depend, in part, upon improvements in the modeling of land surface processes. This requires a good knowledge and extensive description of surface properties at adequate time- and space scales. The Surface Radiation Budget (SRB) components are essential variables for such a description. For instance, large-scale changes in surface albedo can alter the surface energy balance sufficiently to influence surface temperature. This, in turn, might modify the general atmospheric circulation patterns. In particular, surface albedo has been of interest in the Sahel drought problem because of Charney's (1975) hypothesis that increased surface albedo accompanying the reduced rainfall, or human-induced desertification, might exacerbate or even trigger drought.

Satellite data offer a unique opportunity to build the necessary observational base of SRB components. Numerous attempts at estimating surface radiative fluxes from satellite data have been made (e.g., Tarpley 1979; Gautier et al. 1980; Pinker and Ewing 1985; Raschke et al. 1987; Dedieu et al. 1987a; Darnell et al. 1988, 1992; Gupta 1989; Bishop and Rossow 1991; Pinker and Laszlo 1992; Bréon et al. 1994; Rossow and Zhang 1995; Zhang et al. 1995). Recently, global sets of satellite observations from the International Satellite Cloud Climatology Project (ISCCP) became available, allow-

* Current affiliation: Department of Meteorology, University of Maryland at College Park, College Park, Maryland.

Corresponding author address: Dr. Mamoudou B. Ba, Department of Meteorology, University of Maryland at College Park, College Park, MD 20742.
E-mail: mba@atmos.umd.edu

ing implementation of satellite algorithms for the SRB on a global scale in the framework of the World Climate Research Program/SRB project (Whitlock et al. 1995). While these methods give good estimates of downward solar irradiance with the necessary accuracy needed for climatic purposes, important efforts still need to be made in order to have representative estimates of surface albedos. This is not a trivial task because the spectral signature of land surface reflectivity is governed by soil characteristics, vegetation types, and morphology (Dickinson 1983). Numerous satellite estimates of surface albedo over West Africa have been made using quite different methodologies to treat the problems of atmospheric and bidirectional effects. Most ignore the latter problem, producing essentially surface reflectances (e.g., Courel et al. 1984; Pinty et al. 1985; Pinty and Szejwach 1985; Dedieu et al. 1987b; Pinty and Tanré 1987; Pinty and Ramond 1987). In addition, the climatologies that have been produced do not have the adequate resolution to resolve the variability over the African continent, where strong vegetation gradients occur within a few hundred kilometers.

In the present paper (Part I of the series), a methodology to estimate downward surface solar irradiance and surface albedo is described. Meteosat data at 30-km resolution are used. For some applications, this spatial resolution may be more appropriate than the 280-km resolution of the ISCCP and the Earth Radiation Budget Experiment's (ERBE) products (e.g., Darnell et al. 1992; Bréon et al. 1994). Radiometric calibration of the Meteosat visible channel, cloud screening for clear-sky conditions, and corrections of angular variations in surface albedo are detailed. The products are evaluated by comparison with estimates of four major current satellite-based methods. In the companion paper (Part II of the series, Ba et al. 2001), the methodology is applied to variability studies of the surface radiation budget over the African continent.

2. Method of estimating downward solar irradiance and surface albedo

Following Dedieu et al. (1987a), the downward solar irradiance (SW) at the surface can be derived from Meteosat satellite measurements in the 0.35- and 1.1-μm spectral band, using the formula:

$$\mathrm{SW}(t) = E_0(t)\frac{1 - \rho(t)}{1 - \rho_s(t)}, \tag{1}$$

where E_0 is the clear-sky surface solar irradiance over the entire solar spectrum, ρ_s is the surface reflectance, ρ is reflectance of the cloud-surface system, and t is time. The time t corresponds to a viewing geometry of the scene, defined by the sun zenith and azimuth angles, θ_s and ϕ_s and the satellite viewing and azimuth angles, θ_v and ϕ_v. It is assumed that the clear atmosphere (containing molecules and aerosols) is located above the clouds, and ρ, therefore, is the top-of-atmosphere (TOA) reflectance corrected for scattering and absorption by molecules and aerosols [see also Frouin and Chertock 1992)].

Here ρ_s and ρ are the surface and cloud-surface system reflectances in the Meteosat spectral band obtained from the Meteosat equivalent reflectance, ρ^* defined as

$$\rho^*(t) = \pi d^{-2}[E_{\mathrm{sat}} \cos(\theta_s)]^{-1}L^*(t), \tag{2}$$

where E_{sat} is the solar constant in the Meteosat visible/near-infrared spectral band, d is the radius factor (the ratio of actual to mean sun–earth distance), and L^* is the radiance detected by the sensor. The radiance L^* consists of 1) photons reflected by the surface and transmitted from the surface to the sensor, and 2) photons scattered back to space without surface reflection. The apparent reflectance ρ^* can be related to ρ or ρ_s (case of clear sky) using the following formula:

$$\rho^* = t_g\left[\rho_a + \frac{T_a\rho}{(1 - \rho S_a)}\right], \tag{3}$$

where t_g is the gaseous absorption, T_a is the clear-sky diffuse transmittance (due to scattering by aerosols and molecules), S_a is the spherical albedo of the clear atmosphere, and ρ_a is the intrinsic atmospheric reflectance. All the atmospheric functions in Eq. (3) are properly weighted integrals over the Meteosat spectral band (0.35–1.1 μm). They are computed using analytical functions, the Simplified Method for Atmospheric Corrections, Rahman and Dedieu (1994) and are derived from the Simulation of the Satellite Signal in the Solar Spectrum (5S) code (Tanré et al. 1990). The continental aerosol model of the International Radiation Commission (World Climate Research Programme 1983) is used, and aerosol optical depth is set to a constant of 0.23 at 550 nm (23 km of horizontal visibility). The reflectance of the cloud-surface system, ρ, and the surface reflectance, ρ_s, are obtained by inverting Eq. (3). Note that Eq. (3) is strictly valid for a Lambertian lower boundary. The cloud-surface system is obviously not a Lambertian reflector, but the bidirectional characteristics of ρ are unknown (satellite pixels may include clear and cloudy areas in varied proportion), hence our use of Eq. (3).

To compute ρ_s, one must first identify clear-sky conditions. Since clouds are present most of the time, the compositing of clear pixels is necessary over a certain time period. In the present study, ρ_s is determined once a month for each Meteosat observation time (see section 3b). Within such a period the variation of θ_s at a fixed time during the day can be neglected. Thus, the value of ρ_s obtained for each Meteosat observation time is representative of the surface reflectance at the monthly averaged θ_s for that time.

The clear-sky irradiance E_0 in Eq. (1) is evaluated independently of satellite measurements and is given by

$$E_0 = Ed^{-2} \cos(\theta_s)T(\theta_s), \tag{4}$$

where E is the solar constant, and $T(\theta_s)$ is a clear-sky transmission factor, accounting for gaseous absorption mostly by water vapor and ozone, and by molecule and aerosol scattering. Note that the effects of multiple interactions between the clear atmosphere and the surface are neglected in Eq. (4). Recent satellite measurements (e.g., Ramanathan et al. 1989) show that E is about 1363–1372 W m^{-2}. A value of 1372 W m^{-2} is used in the present study.

Climatologies of vertically integrated water vapor content (Tuller 1968) and vertically integrated ozone content (London et al. 1976) obtained for 10° latitudinal zones and each month of the year are used to compute the contribution to T of water vapor and ozone according to Darnell et al. (1988). Absorption due to oxygen and carbon dioxide is computed using Yamamoto's (1962) formulas.

Scattering by aerosols is computed with the same aerosol model and optical thickness used for T_a in Eq. (3), that is, the continental model of the International Radiation Commission and 0.23 at 550 nm. By fixing aerosol conditions, variability due to dust and biomass burning events is not accounted for. However, comprehensive information about aerosols over Africa is lacking. Measurements have been limited in space and time, and few cover the period of our satellite analysis. The studies of ben Mohamed and Frangi (1983, 1986), Fouquard et al. (1987a,b), and Pinker et al. (1994) describe point measurements, limited to one station. Those of Cerf (1980), d'Almeida (1986, 1987), Holben et al. (1991), and Faizoun et al. (1994) provide some spatial information, as they report on 2 to 11 stations. In some cases, measurements are limited to a few months; in most cases, they cover a 1- or 2-yr period at each station. All of the above studies have revealed a high spatial and temporal variability of aerosol characteristics (type, optical thickness), even on a day-to-day basis. Thus one could introduce substantial errors by attempting to use the results of these studies. The chosen optical thickness of 0.23, on the other hand, is on the lower end of expected values. Note that, the cloud-filtering procedure (section 3b) tends to select days with the lowest aerosol burden.

In the parameterization of SW for a cloudy atmosphere, molecular scattering and gaseous absorption are considered as in the clear-sky case, but cloud absorption is neglected. This assumption is made because pixel composition is unknown (see Dedieu et al. 1987a). As mentioned earlier, the effects of clouds and of the clear atmosphere are decoupled. Cloud optical thickness is generally the governing parameter in cloudy conditions, but neglecting the relative location of clouds, molecules, and aerosols in the vertical may not be realistic in some cases. In the absence of information about cloudiness distribution within the satellite pixels, a more complex parametrization of cloud effects is not attempted. The simplified treatment of clouds seems to be warranted by the performance of the model that produced better results rather than more complicated schemes (Whitlock et al. 1990). The daily mean of downward solar irradiance Sw_d, is obtained by integrating Eq. (1) between sunrise and sunset times and is given by

$$\mathrm{SW}_d = \int E_0(t)\frac{1 - \rho(t)}{1 - \rho_s(t)}\,dt. \tag{5}$$

Numerical integration is performed by summing the values obtained at each METEOSAT observation. For each observation time, E_0 is evaluated over a time interval centered at the time of that observation and multiplied by the term $[1 - \rho(t)]/[1 - \rho_s(t)]$ to account for cloud attenuation.

The daily mean surface reflectance, ρ_{s_d}, cannot be obtained by simply averaging the instantaneous values of $\rho_s(t)$; it must be weighted by the solar irradiance reaching the surface (SW), that is,

$$\rho_{s_d} = \frac{\int \mathrm{SW}(t)\rho_s(t)\,dt}{\int \mathrm{SW}(t)\,dt}. \tag{6}$$

Using Eq. (1), ρ_{s_d} is therefore computed as

$$\rho_{s_d} = 1 - \frac{\int E_0[1 - \rho(t)]\,dt}{\int \mathrm{SW}(t)\,dt}. \tag{7}$$

Equation (7) and therefore ρ_{s_d}, averages some of the bidirectional variability in surface reflectance. This variability may be large, depending on the type of surface (e.g., Kriebel 1978; Kimes 1983; Deering 1989; Gutman 1992; Ba et al. 1995). The degree of variability is unknown, however, especially for nonhomogenous pixels, thus, preventing the use of ancillary information on bidirectional effects of natural surfaces to complement Meteosat observations and to compute an accurate daily mean surface albedo A_{s_d}. However, the relatively large field of view of the sensor tends to reduce the angular effects, and ρ_{s_d} obtained from Eq. (7) may be considered representative of A_{s_d}. This albedo still depends on solar geometry since the daily mean of $\cos(\theta_s)$ varies during the year. In order to study the seasonal variations of surface albedo properly, that is, independently of geometric effects, this dependency must be minimized (see section 3c).

3. Data processing

Meteosat data in the ISCCP B2 format are used in the computations. These data are obtained from the European Satellite Operation Center (ESOC). They contain 3-h, 8-bit digitized images in three spectral bands: 0.4–1.1 (visible channel), 10.5–12.5 (thermal infrared chan-

nel), and 5.7–7.7 μm (water vapor channel). During the period of study, July 1983–July 1988, Meteosat data are available for all months except December 1983 and July 1987.

A Meteosat B2 image has 30-km spatial resolution and is obtained by sampling the original full resolution (about 5 km at nadir) image every six rows and six columns. All images are geometrically corrected and navigated to a fixed reference. In the validation analysis, the surface albedo and downward solar irradiance (*SW*) products of Pinker and Staylor (Whitlock et al. 1995), Darnell et al. (1992), and Bishop and Rossow (1991) are used. These products are mapped to the ISCCP equal-area grid with approximate dimensions of 278 km $\times$ 278 km (2.5° latitude $\times$ 2.5° longitude). For comparison, the Meteosat products (SW and surface albedo) are degraded from 30-km resolution by averaging all pixels contained within each of the 2.5° $\times$ 2.5° ISCCP grid boxes.

The Meteosat data processing involves the following steps: 1) calibration of raw digital counts, providing TOA radiances; 2) normalization of radiances by solar irradiance, to compute TOA reflectance; 3) cloud screening using a minimum shortwave reflectance (0.35–1.1 μm) compositing technique (Arino et al. 1991); 4) correction of atmospheric effects based on climatologies (Rahman and Dedieu 1994); and 5) correction of θ_s effects on estimated surface albedo. Steps 2 and 4 are described above (section 2). In this section, radiometric calibration, cloud screening, and correction of θ_s effects on the estimated surface albedo are detailed.

a. Radiometric calibration

The Meteosat data used in the present study are in the form of digitized 8-bit counts. The radiance L^* detected by the satellite is a linear function of the numerical count and is calculated by

$$L^* = \alpha(\mathrm{CN} - \mathrm{CN}_0), \tag{8}$$

where CN is the satellite numerical count, CN_0 is the space count, and α is a calibration factor expressed in W m^{-2} sr^{-1} count^{-1}. The calibration factor changes over time due to exposure to the space environment and the aging of the optical system. Consequently, monitoring the temporal stability of the detected signal, that is, of α, is necessary.

For this study, ISCCP calibration coefficients (Brest and Rossow 1992; Desormeaux et al. 1993) are used to adjust the radiance obtained from Eq. (8). These coefficients are obtained by comparing Meteosat measurements with those of the Advanced Very High Resolution Radiometer (AVHRR) on board the National Oceanic and Atmospheric Administration (NOAA) satellites.

The calibration procedure is done in two steps (see Desormeaux et al. 1993). First, radiances are normalized by those sensed by AVHRR at the same time and location with the same viewing geometry. This normalization procedure uses ocean and clouds as constant-radiance targets. Only thick and solid overcast cells (50 km $\times$ 50 km) having optical depths above 80 are selected. The normalization procedure allows for the correction of relatively slow changes (timescale of the order of 1 month). Second, the time history of the radiance distribution in each image of the series is examined to detect sudden, systematic changes that exceed some minimum magnitude. Short-term changes are detected by analyzing two-week records of the radiance distribution for each whole image, represented by the mean value, plus and minus one standard deviation, together with the 10th, 25th, 50th, 75th, and 90th percentile values. A time series of radiance distribution statistics over several years is used to determine the lowest variability that occurs in the lower percentile values. This lowest variability includes real variations in ocean surface reflectance, and is less than 2% in ocean reflectance (Desormeaux et al. 1993). Values of 2% in ocean reflectance are used as conservative limits. Small adjustments are performed as necessary whenever the variability in the lowest percentile (10th) exceeds 2% in ocean reflectance. After correction, and normalization by solar irradiance, the Meteosat radiance becomes

$$L_n^* = A\frac{\pi L^*(t)}{E_{\mathrm{sat}}} + B \tag{9}$$

and ρ^* is obtained from L_n^* as:

$$\rho^* = d^{-2}\cos(\theta_s)^{-1}L_n^*. \tag{10}$$

The performance of the ISCCP calibration is examined over test sites in the Libyan desert (24°–25°N, 12°–13°E), the Ténéré desert (17.5°–18.5°N, 10.5°–11.5°E), and eastern Mauritania (19.5°–20.5°N, 9.5°–10.5°W). The site in Libya is primaily selected because it exhibits a good spatial uniformity, a high reflectance (>0.40) allowing minimization of the atmospheric effects, a temporal stability, and a low-cloud-coverage frequency (Arino et al. 1991). The two other desert sites are used to verify the calibration adjustment made using the Libyan site.

If the calibration coefficients were correct, we would expect little interannual variability in the TOA reflectance of the test site. An analysis of the Meteosat reflectances shows otherwise and the examination of the time series of digital count and calibration coefficient, *A*, suggests a problem with the ISCCP calibration.

The time series of clear-sky digital counts, corresponding to observations at 1130 UTC are shown in Fig. 1a. Most evident is the month-to-month variability, a manifestation of the changing conditions of solar radiation during the course of the year. However, there is also a significant increase in the Meteosat signal after May 1987. In general, the signal presents small variations during the other years, which may be caused by atmospheric constituents. The large signal increase from April 1987 to May 1987 is a consequence of a gain

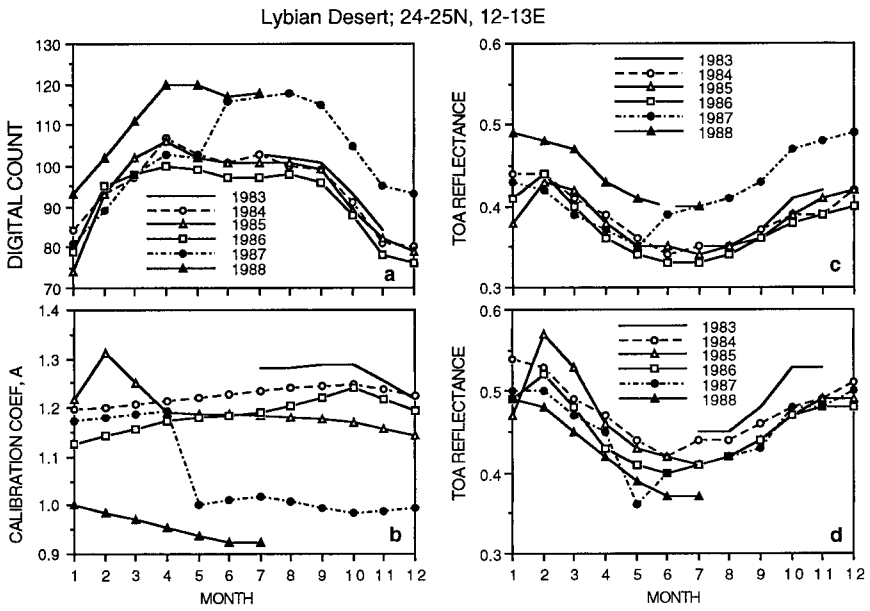

FIG. 1. Monitoring of the Meteosat 2 solar channel over the Libyan desert site. (a) Time series of clear-sky digital count, (b) time series of the ISCCP calibration coefficients A, (c) time series of TOA reflectance computed with ESOC calibration, and (d) time series of TOA reflectance computed with ISCCP calibration applied.

change in the visible channel of Meteosat 2 (Rossow et al. 1992).

The time series of the ISCCP calibration coefficient, *A,* are generally consistent with those of the clear-sky data (Fig. 1b). One expects that the decrease in the satellite signal will correspond to an increase in *A,* indicating a degradation in instrument response. The large increase in *A* from January to February 1985, however, is not followed by a decrease in the satellite signal, indicating that the calibration may be incorrect.

The degradation rate of the satellite sensor generally results in a lower satellite signal (digital count). A signal increasing with time does not usually occur unless there are onboard temperature variations or gain changes from ground controllers. There was a gain change in the visible channel in May 1987 that explains the larger digital counts from June 1987 to July 1988. This is consistent with the decrease in *A* and in the calibration coefficient obtained by Moulin et al. (1994). The ISCCP coefficient, *A,* decreases from a value of 1.19 in April 1987 to 1.00 in May 1987.

Figure 1c displays the TOA reflectance computed with the ESOC calibration, that is, without ISCCP correction. The temporal fluctuations of the TOA reflectance are quite similar to those of the clear-sky digital count (Fig. 1a).

When the monthly ISCCP calibration coefficients are used (Fig. 1d), significant fluctuations appear in the TOA reflectance, particularly in February 1985 and May 1987. These fluctuations are correlated to those of the calibration coefficients. For instance, the TOA reflectance like, *A,* is generally much lower in 1988 than during the other years. We also notice the conspicuous drop in TOA reflectance in May 1987, associated with a lower *A.* These large changes in TOA reflectance are not due to surface property changes, but to calibration uncertainties. A comparison of thick-cloud albedos normalized to the *NOAA-9* values for selected months revealed that ISCCP geostationary satellite calibrations are accurately normalized to within 5% of the polar orbiter during the *NOAA-9* period. However, some values differ by more than 5% (see Whitlock et al. 1995). These large errors may be the result of inaccuracy in the cloud albedo determination and/or the effects of cloud changes; cloudy radiances generally exhibit significant variations at both small spatial and temporal scales (clear radiances are generally much less variable). This may be the cause of the year-to-year fluctuations found here in calibrated TOA reflectances.

Brest et al. (1997) provided updated radiance calibrations for ISCCP. Using the new calibration coefficients, the year-to-year changes over the stable targets did not disappear, although a definite improvement was noticed for some years (e.g., 1983). Calibration adjustment of old or new coefficients, therefore, is necessary to eliminate the artificial changes. We chose to work with the old coefficients, but similar results would have been obtained by adjusting the recent values.

To make Meteosat observations comparable from one year to another, the calibration factor must adequately compensate for all changes in the detected signal due to sensor degradation. Therefore an adjustment factor, ε, is computed to correct on a month-to-month basis, the TOA reflectance that exhibits a significant departure

TABLE 1. Monthly adjustment factors, ϵ, computed using the Libyan Desert as a target of constant reflectance. When $\epsilon = 0$, no adjustment is made. Stars indicate that no Meteosat data were available to compute ϵ.

	1983	1984	1985	1986	1987	1988
Jan	*	0	0	0	0	0
Feb	*	0	0.106	0	0	−0.062
Mar	*	0	0	0	0	−0.044
Apr	*	0	0	0	0	−0.076
May	*	0	0	0	−0.145	−0.075
Jun	*	0	0	0	0	−0.122
Jul	0.087	0.063	0	0	*	−0.085
Aug	0.064	0.056	0	0	0	*
Sep	0.100	0.052	0	0	0	*
Oct	0.119	0	0	0	0	*
Nov	0.094	0	0	0	0	*
	*	0	0	0	0	*

from the long-term mean (1983–88). More precisely, the adjustment factor is defined as

$$\varepsilon = \frac{\rho^* - \rho^*_{\text{av}}}{\rho^*_{\text{av}}}, \tag{11}$$

where ρ^* is the monthly TOA reflectance computed using the ISCCP calibration and ρ^*_{av} is the monthly TOA reflectance, also computed using the ISCCP calibration, but averaged over the years that do not exhibit large departure from the long-term mean. The adjustment factors determined over the Libyan site are listed in Table 1. Using these adjustment factors, the TOA reflectance, ρ^* computed using the ISCCP calibration [Eqs. (9) and (10)], is modified as

$$\rho^*_{\text{corr}} = \rho^* - \varepsilon\rho^*. \tag{12}$$

Figure 2 displays time series of the TOA reflectance corresponding to two other desert sites (Ténéré, Mauritania) before and after applying Eq. (12). As can be seen, the large fluctuations due to calibration errors (Figs. 2a and 2b) are dramatically reduced (Figs. 2c and 2d). In the present study, all TOA reflectances computed using the ISCCP calibration are modified according to Eq. (12). The accuracy of the adjustments for precise intercomparisons may be questioned, but the computed surface albedo values over the Sahara desert show very little interannual variability, as would be expected (see Part II).

b. *Cloud- and large optical depth screening procedures*

In Eq. (1), ρ_s must be determined. This is not a trivial task because clear and cloudy conditions are not always easy to distinguish. Moreover, large aerosol optical depths must be eliminated when computing the surface reflectance. Therefore, a good cloud-screening technique would be one that not only eliminates the cloudy conditions, but also the hazy ones and cloud shadows.

Selecting a minimum reflectance over a period of time, one can eliminate the cloudy conditions because clouds are generally more reflective than the underlying surface. However, this approach tends to favor some particular atmospheric conditions. In the presence of absorbing aerosols, the reflectance of bright surfaces may be underestimated (Legrand et al. 1985, 1988). On the other hand, using the highest thermal infrared (IR) signal efficiently eliminates large aerosol optical depth observations, but may fail to discriminate the presence of low clouds with high temperature, as these are usually present over tropical forests and highlands.

In this study, following Arino et al. (1991), a combination of both IR and visible methods is used over a monthly period to optimize the cloud-screening procedure. This combination addresses the main problems encountered: large optical depth in the case of the visible method and low clouds in the case of the IR method. First, we use the maximum IR measurement over a 10-day period within the month to select 3 days during the month. Then, we use the visible criteria to select the minimum reflectance value out of these 3 days to identify the day least affected by atmospheric conditions.

While visually examining some of the composite images obtained by the above procedure, we noticed that the technique sometimes failed to eliminate low clouds. Therefore, we used a reflectance threshold of 0.15, corresponding to the high limit of spatial variability of surface reflectance for a given month. This threshold is defined as the ratio (r_0) of the standard deviation to the mean computed from nine pixels encompassing a given pixel. It is empirically set after examining the possible values of r_0 corresponding to clear-sky conditions over the entire image. Whenever r_0 is greater than the threshold (cloud contamination), the day corresponding to the minimum reflectance value selected over the entire month is chosen as the month's lowest optical depth. This problem illustrates the limitation of the cloud-screening technique in regions frequently covered by low and warm clouds. The ability of the technique to screen large optical depths was tested by Arino et al. (1991) using optical depth observations at two sites in Burkina Faso. Their results showed that the satellite clear-sky measurements as obtained by the technique during a period of one month do not always correspond

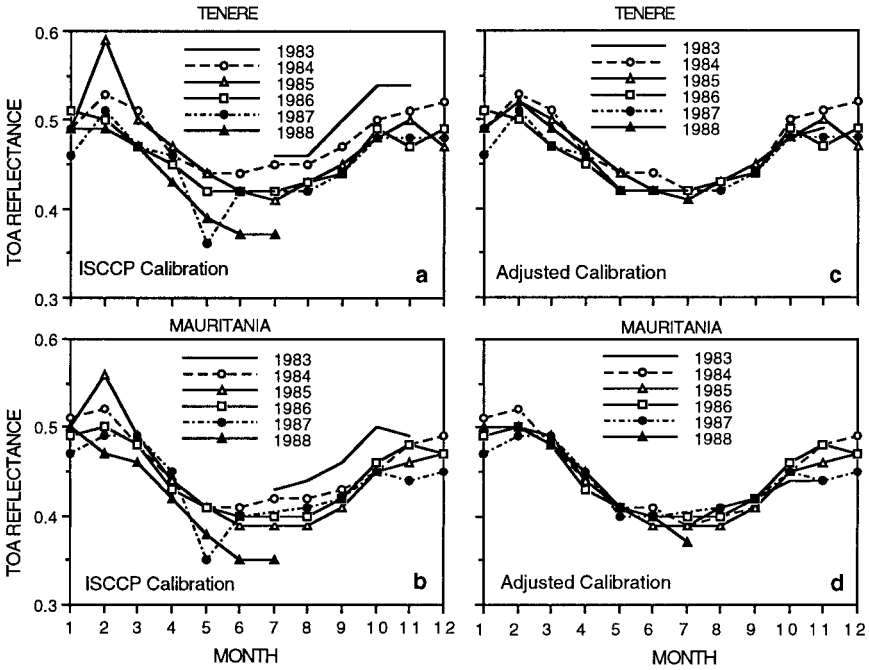

FIG. 2. Time series of TOA reflectance over the Ténéré Desert, and northeastern Mauritania. (a), (b) TOA reflectance computed using ISCCP calibration coefficients; (c), (d) TOA reflectance adjusted using the ε factor (see text).

to the smallest aerosol optical depth measured over the same period. Therefore, the spatially and temporally invariant value of 0.23 for aerosol optical depth sometimes underestimates aerosol effects in regions with a high frequency of dust storms such as the Sahel and the Sahara.

c. Correction of the sun zenith angle effects on estimated surface albedo

The daily mean of surface reflectance, ρ_{s_d}, computed using Eq. (7) to estimate the daily mean of surface albedo, A_{s_d}, is retrieved from the Meteosat solar radiance by removing atmospheric effects. Even though surface bidirectional effects are averaged (see section 2b), the surface albedo as retrieved from Eq. (7) is still dependent on the sun zenith angle, θ_s. Figure 3a displays the spatial distribution of regression statistics between monthly means of surface albedo and $\sec(\theta_s)$ using a linear relationship. This relationship, used to account for the effect of the sun zenith angle on surface albedo, is written as follows:

$$A_s = A_{s0} + b\frac{1}{\cos(\theta_s)}, \tag{13}$$

where A_s is the corrected surface albedo. Monthly means of the surface albedo averaged over the period 1983–88 were used to compute the coefficients A_{s0} and b.

Shaded areas in Fig. 3b represent regions where the determination is statistically significant at the 99% confidence level. The correction of the surface albedos for θ_s effects is only performed in these regions. Elsewhere, the level of statistical significance is not satisfactory; other factors may contribute more to seasonal variations of surface albedo.

It is important to note that the angular correction [Eq. (13)] does not distinguish between actual angular effects and seasonal changes in surface characteristics. In deserts and rain forests, however, the surface characteristics vary little during the course of the year, and the seasonal variations in surface albedo are mostly due to solar geometry effects. In semiarid regions such as the Sahel, on the other hand, surface texture and structure change dramatically from wet to dry seasons; but the vegetation cycle is short (3–4 months) and the correlation with sun zenith angle, which does not change much, is low. Consequently, as shown in Fig. 3, the θ_s effects are large in regions with a stable surface such as deserts and forests, and the correction is essentially applied to these regions.

4. Sensitivity tests

Arino et al. (1992) reported on the accuracy of surface reflectance determined from Meteosat data. Their error analysis identified three main problems: calibration uncertainty, atmospheric corrections, and spectral and directional effects of the surface. They concluded that calibration inaccuracy is within 10%, which may cause relative errors in the surface reflectance of 10%. Spectral

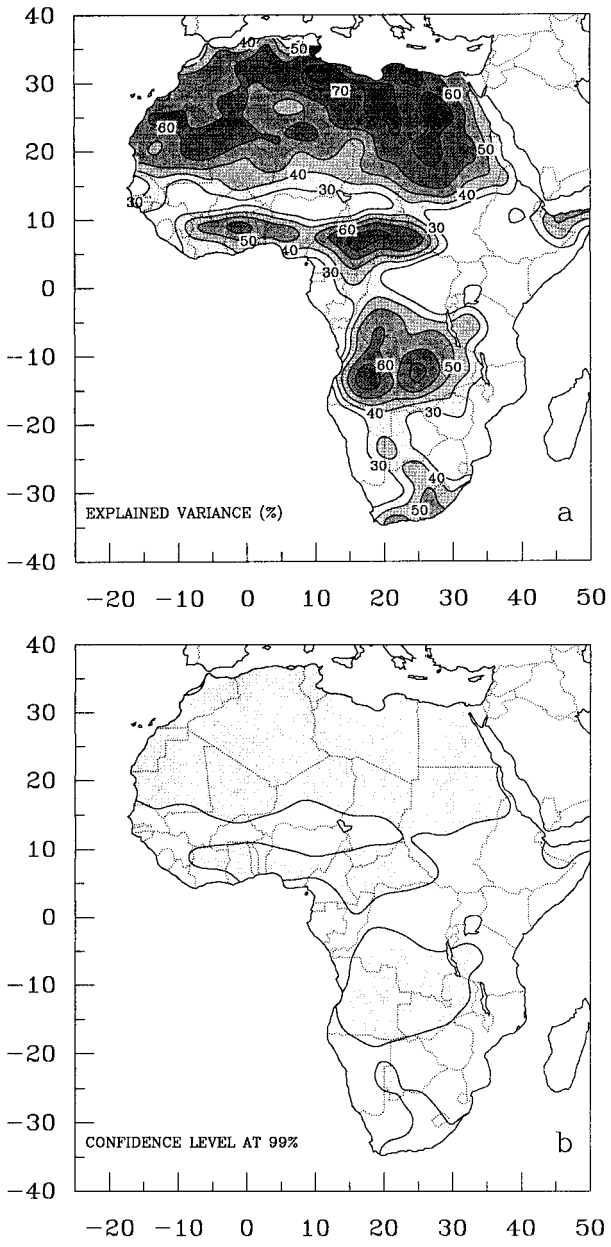

FIG. 3. Spatial distribution of regression statistics between computed surface albedos and sec(θ_s): (a) explained variance (%), and (b) statistical significance at the 99% confidence level (shaded areas).

effects may account for a maximum bias of 0.01 in the reflectance of a vegetated surface, and directional effects can lead to a bias of 0.035 between surface reflectance estimates made from two observations taken at different times. The maximum reflectance error due to the atmosphere was estimated to be on the order of 0.03 and 0.01 for surface reflectances of 0.40 and 0.10, respectively. Similar errors are expected in the monthly surface albedo.

The sensitivity of the algorithm to input data, specifically water vapor and aerosol amounts, is investigated. Three different sites are selected. The first site is located in the Libyan Desert (24.5°N and 12.5°E) and has a high surface albedo of 0.50. The second site is located in northern Burkina Faso (Dori: 14.05°N and 0°) and has a surface albedo around 0.30. The third site is located in southern Burkina Faso (Fada Ngourma: 12.06°N and 0.4°E) and has a surface albedo of 0.20. Monthly downward surface solar irradiance and surface albedo are computed at each of these three sites for January and July 1986. The climatological value of the water vapor amount and a standard value of 0.23 for aerosol optical thickness at 550 nm are varied by ±25%. A large optical thickness (0.8), a value frequently observed at Niamey during the dry season (ben Mohamed et al. 1992; N'Tchayi et al. 1997), is also used. The results of the sensitivity tests are summarized in Table 2, which gives the difference between calculated quantities obtained by increasing and decreasing input data by 25%.

When the water vapor amount is varied over the range [−25%, 25%], the downward solar irradiance decreases by 11–23 W m^{-2}, less than 10% of the value computed using the climatological water vapor amount. The largest differences between January and July 1986 are observed for the Libyan site (12 W m^{-2}), while the differences between these two months are only 5–7 W m^{-2} for the Burkina Faso sites. The differences in surface albedo are 0.01 for Fada Ngourma and Dori and 0.02 for the Libyan site, representing a decrease of 5%, 4%, and 4%, respectively, in the value computed with the climatological of water vapor amount.

When the optical thickness τ_a is varied by ±25% around 0.23, the downward solar irradiance decreases by 7–9 W m^{-2}. When τ_a is 0.8 instead of 0.23, the decrease is more pronounced, with values ranging from 25 to 46 W m^{-2}. In general, the sensitivity to τ_a is higher in January, because of the larger optical path during that month. However, compensatory effects may occur in some situations. A high τ_a gives a higher estimate of aerosol-scattering effects, resulting in a lower cloud reflectance. The lower cloud reflectance, in turn, tends to compensate the effect of higher τ_a on atmospheric transmission.

For surface albedo, the difference between values computed for (τ_a + 25%τ_a) and (τ_a − 25%τ_a) is 0.01 and 0.02. With a much higher value of τ_a (0.8), the difference is large when surface albedo is high (i.e., 0.08–0.13 for the desert site). Such high τ_a values are observed in desertic regions (ben Mohamed et al. 1992). However, as mentioned above (section 3b) the cloud-filtering procedure tends to select days with the lowest τ_a values, reducing the errors obtained by using a τ_a value of 0.23. The figures given in Table 2 for the effect on surface albedo of increasing τ_a to 0.8 probably represent maximum errors due to uncertainties in τ_a.

TABLE 2. Sensivity of monthly downward solar irradiance and surface albedo to water vapor amount (WV) and aerosol optical depth (τ_a). Tests are performed for Jan and Jul 1986 at three locations in the Libyan Desert and Burkina Faso.

	Jan		Jul	
	ΔSW (W m^{-2})	ΔA_S	ΔSW (W m^{-2})	ΔA_S
Libyan Desert (25.5°N–12.5°E)				
(WV + 25%) − (WV − 25%)	−11	0.02	−23	0.02
(τ_a + 25%) − (τ_a − 25%)	−6	0.02	−10	0.01
(τ_a = 0.8) − (τ_a = 0.23)	−25	0.13	−43	0.08
Dori: Burkina Faso (14.05°N–0°)				
(WV + 25%) − (WV − 25%)	−15	0.01	−22	0.01
(τ_a + 25%) − (τ_a − 25%)	−7	0.01	−5	0.02
(τ_a = 0.8) − (τ_a = 0.23)	−29	0.06	−46	0.03
Fada Ngourma: Burkina Faso (12.06°N–0.4°E)				
(WV + 25%) − (WV − 25%)	−16	0.01	−21	0.01
(τ_a + 25%) − (τ_a − 25%)	−7	0	−10	0
(τ_a = 0.8) − (τ_a = 0.23)	−30	0.02	−46	0.01

5. Product evaluation

a. Comparison with other satellite products

The present algorithm is compared with four satellite algorithms, those of Pinker and Staylor (Whitlock et al. 1995), Darnell et al. (1992; hereinafter referred to as Darnell), and Bishop and Rossow (1991; hereinafter referred to as Bishop). These algorithms are based on radiative transfer models and use ISCCP C1 data. In the C1 format, the satellite data are mapped to the ISCCP equal-area grid that has approximate dimensions of 278 km × 278 km (2.5° latitude × 2.5° longitude; Whitlock et al. 1995). All four algorithms have been evaluated against measurements of downward surface solar irradiance. For the purpose of the present comparison, the products obtained with Meteosat B2 are degraded by averaging all pixels contained within each of the 2.5° × 2.5° ISCCP grid boxes. Coastal area pixels are not considered because our estimates are only made over land. Furthermore, only data for January 1986–88 and July 1985–86 are used, since at the time of the study the Staylor and Pinker results were only available for these years.

Table 3 summarizes the comparison statistics of downward surface solar irradiance and surface albedo estimates by various satellite algorithms, and Figs. 4 and 5 display the corresponding scatterplots. The agreement is good between our results and those of Darnell and Staylor, for both variables. The statistics are similar, which is not surprising since the Darnell and Staylor algorithms are both a modified version of an earlier algorithm by Darnell et al. (1988). For downward solar irradiance, the biases are less than 2 W m^{-2} and the rms errors (root-mean-square errors with respect with the best-fit line) less than 12 W m^{-2}. For surface albedo, the biases are between −0.01 and 0.02 and the rms errors are less than 0.04. Bishop's estimates of downward solar irradiance, on the other hand, are system-

TABLE 3a. Comparison statistics between the various satellite algorithms for downward solar irradiance.

	Jan 1986–88 NBP = 819			Jul 1985–86 NBP = 546		
	Correlation coefficient (R)	Rmse (W m^{-2})	Bias (W m^{-2})	Correlation coefficient (R)	Rmse (W m^{-2})	Bias (W m^{-2})
This study vs						
Darnell	0.97	8	1	0.97	12	−1
Staylor	0.96	10	−1	0.98	11	−2
Pinker	0.91	14	1	0.92	21	1
Bishop	0.94	13	−21	0.98	10	−24
Darnell vs						
Staylor	0.99	4	2	0.99	3	1
Pinker	0.95	16	−1	0.96	12	−2
Bishop	0.97	10	−22	0.98	8	−23
Staylor vs						
Pinker	0.96	11	2	0.94	15	3
Bishop	0.98	8	−20	0.98	8	−22
Pinker vs						
Bishop	0.95	16	−22	0.95	14	−25

TABLE 3b. Comparison statistics between the various satellite algorithms for surface albedo.

	Jan 1986–88 NBP = 819			Jul 1985–86 NBP = 546		
	Correlation coefficient (R)	Rmse	Bias	Correlation coefficient (R)	Rmse	Bias
This study vs						
Darnell	0.95	0.04	0.02	0.94	0.03	−0.01
Staylor	0.93	0.04	0.02	0.94	0.03	−0.02
Pinker	0.71	0.10	0.07	0.90	0.04	0.0
Bishop	0.97	0.03	0.15	0.97	0.02	0.10
Darnell vs						
Staylor	1	0	0	0.99	0.02	0
Pinker	0.79	0.07	0.05	0.90	0.05	0.02
Bishop	0.94	0.04	0.12	0.95	0.04	0.11
Staylor vs						
Pinker	0.78	0.07	0.05	0.91	0.04	0.02
Bishop	0.94	0.03	0.13	0.95	0.04	0.12
Pinker vs						
Bishop	0.75	0.07	0.08	0.91	0.05	0.09

atically biased high by 21–24 W m^{-2} for both January and July with rms errors less than 3 W m^{-2} (Table 3a). The surface albedo estimates are also largely biased compared to our estimates (Table 3b); the bias is 0.15 in January and 0.10 in July. The correlation coefficient, however, is high, 0.97 for both January and July. Note that Bishop's values represent albedos in the visible (0.6 μm) whereas our values represent albedos in a broader spectral range (0.4–1.1 μm). Such a high correlation between broadband and narrowband albedos has been reported by Arino et al. (1992). In January, our estimates of downward solar irradiance are lower for vegetated regions and higher for arid and semiarid regions when compared with Pinker's values (Fig. 4). The correlation is much better in July (Tables 3a,b), but Pinker's values are still much lower for albedos above 0.20.

The reasons for differences between our estimates of downward solar irradiance and those of Darnell, Staylor, Pinker, and Bishop are not established. However, part of the differences might be due to the surface albedo used as input to the various downward solar irradiance algorithms. Pinker's radiative transfer model specifies the spectral dependence of surface reflectance in the target grid using the vegetation map of Matthews (1983). A narrowband-to-broadband transformation and an anisotropic correction are then applied. Similarly, Bishop's radiative transfer model uses the area-weighted average of spectral ratios for eight vegetation types (with seasonal adjustments); land ice, sea ice, and fresh snow. Over the African continent, the model uses a surface reflectance corresponding to the ISCCP surface visible (0.6 μm) reflectance, which is an area-averaged reflectance. The near-infrared reflectance is derived from the visible reflectance. By contrast, Darnell's and Staylor's albedos are based on angularly corrected, broadband ERBE clear-sky satellite data. These are more comparable with those obtained from the Meteosat solar band.

b. Comparison with ground-based measurements

The Meteosat estimates of monthly downward surface solar irradiance are compared with surface measurements from the African pyranometer network. All the 1986 data available from the various reporting stations [670 measurements from 64 stations in 11 countries compiled by DiPasquale et al. (1996)], are used in the comparison. In Fig. 6, the ground-based measurements are plotted against the satellite-derived estimates. The overall performance statistics are good, with a correlation coefficient of 0.75, a small bias of 3 W m^{-2}, and a standard deviation of 29 W m^{-2} (about 12% of the mean). For some countries, however, the correlation coefficient is low and the differences between measurements and estimates are large and systematic (Table 4). In the case of Sudan and Zaire, for example, the correlation coefficient is less than 0.5. The largest bias, 50 W m^{-2} (28%), is observed for Ghana, but only one station reported data.

Seasonal variations over the year of 1986 are examined at six selected stations around the continent (Fig. 7): Cairo (Egypt), the Island of Réunion, Bambey (Senegal), Casablanca (Morocco), Bulawayo (Zimbabwe), and Nairobi (Kenya). The best agreement is obtained for the Cairo station, where satellite estimates and surface observations are well correlated during all months. A large bias (overestimation) exceeding 50 W m^{-2} is observed for some months (May–July) at the Bambey and Casablanca stations. At the Southern Hemisphere stations, on the contrary, satellite estimates tend to be lower than the measurements. Nevertheless, the overall comparison of the six stations shows that the satellite

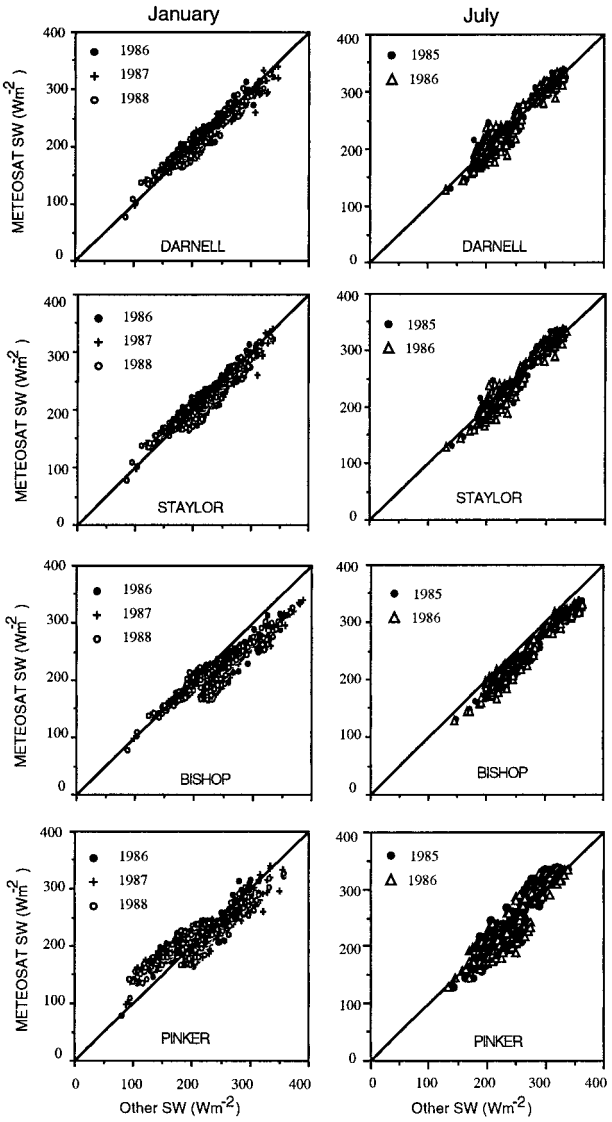

FIG. 4. Comparison of downward surface solar irradiance obtained in the present study with that of Darnell, Staylor, Bishop, and Pinker during Jan 1986–88 (left) and Jul 1985–86 (right).

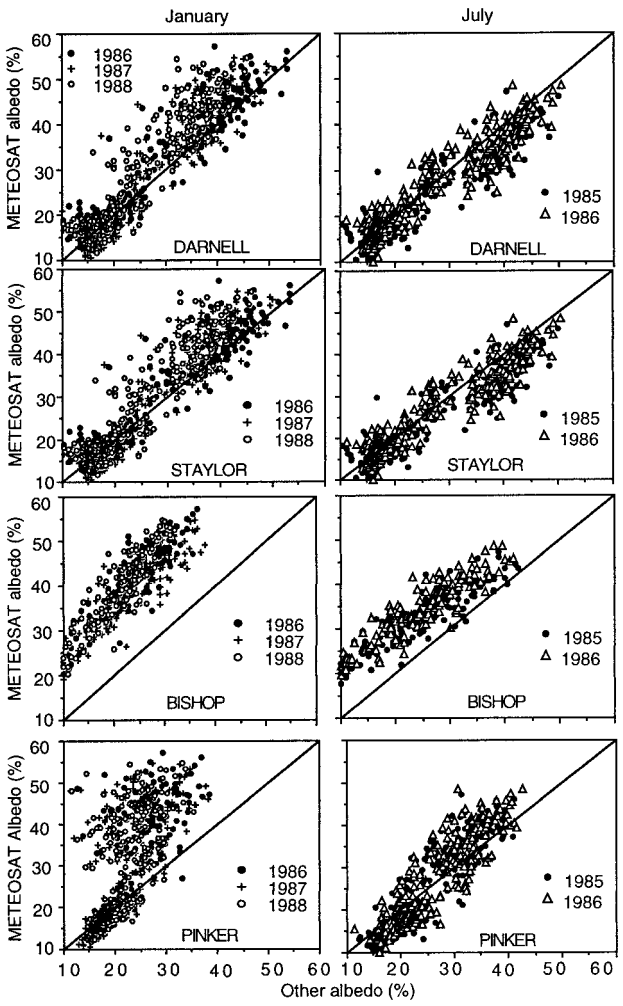

FIG. 5. Comparison of surface albedo obtained in the present study and that of Darnell, Staylor, Bishop, and Pinker during Jan 1986–88 (left) and Jul 1985–86 (right).

estimates reproduce adequately the seasonal evolution of downward surface solar irradiance at these stations.

The overestimation of downward surface solar irradiance by the satellite at Bambey and Casablanca might be due to a too large clear-sky transmittance (i.e., a too small aerosol optical depth). The value of 0.23 for τ_a is not adequate in dry regions such as the Sahel (i.e., large biases in Senegal) where dust storms are frequent; Saharan dust may also affect the Moroccan coast. According to the sensivity tests (section 4), the water vapor amount would have to be underestimated by about 100% to explained the discrepancies, which is not realistic. The underestimation by the satellite at the stations located south of the equator, on other hand, cannot be explained by the aerosol optical depth of 0.23 (even

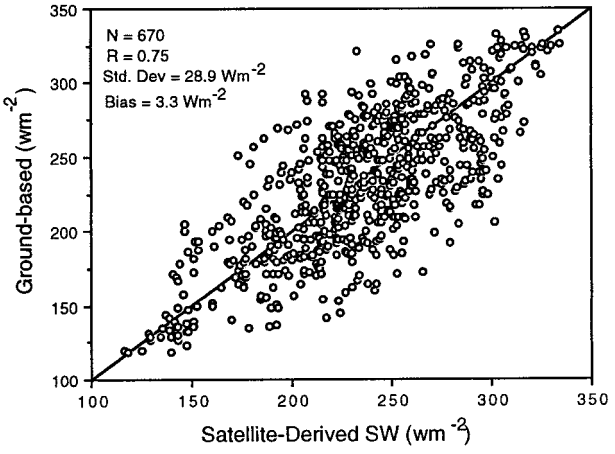

FIG. 6. Ground-based vs satellite-derived estimates of monthly downward solar irradiance. The 1986 measurements from 64 stations in 11 African countries are used in the comparison.

TABLE 4. Statistics of measured vs estimated monthly downward solar irradiance at 64 African stations in 1986.

Country	No. of stations	No. of points	Correlation coefficient (R)	Bias	Rmse (W m^{-2})	Obs mean (W m^{-2})
Egypt	9	108	0.98	1.4	11.5	236.2
Senegal	8	64	0.76	36.1	18.8	223.3
Sudan	13	103	0.48	19.9	24.5	243.5
Zimbabwe	2	22	0.87	−11.6	13.3	229.2
Morocco	1	11	0.97	11.4	18.0	209.9
Kenya	11	142	0.59	−17.3	22.2	250.2
Mozambique	12	131	0.83	−16.4	21.6	230.6
Ghana	1	10	0.85	52.0	12.1	177.8
Nigeria	1	12	0.83	30.4	14.5	191.4
Réunion	1	12	0.98	−16.0	8.3	229.0
Zaire	5	55	0.33	31.5	16.6	187.3
All	64	670	0.75	3.3	28.9	231.5

decreasing the value to zero would not be sufficient to explain the discrepancies). The climatological values of water vapor amount, however, might be too high at those stations. Further interpretation of the discrepancies is difficult, and may not be possible until the accuracy of the surface observations is established.

6. Discussion and conclusions

The model used to compute downward surface solar irradiance and albedo is based on several simplifying assumptions. First, the effects of clouds and the clear atmosphere are decoupled. Second, in the parameterization of downward surface solar irradiance, clouds are considered nonabsorbing. Third, the spectral dependency of the cloud–surface system is not taken into account. Fourth, the bidirectional characteristics of the cloud system are neglected when correcting the effects of atmospheric gases and aerosols. The good agreement between estimates from models accounting for cloud absorption and bidirectional effects (e.g., Darnell et al. 1992), and using broadband satellite measurements, suggests that these assumptions are reasonable at least on a monthly timescale.

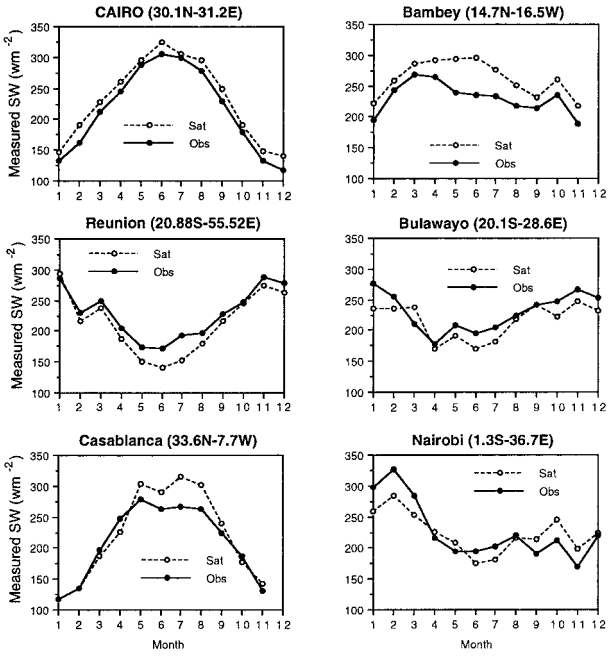

FIG. 7. Time series of measured (solid line) and estimated (dashed line) downward surface solar irradiance for six individual African stations.

Uncertainties in some input variables, namely, aerosol optical thickness and water vapor amount, on the other hand, may have a significant impact on the accuracy of the estimates. The aerosol optical depth of 0.23, in particular, is not adequate for most days in semiarid and arid regions such as the Sahel and the Sahara Desert. These regions experience frequent dust storms, making it necessary to use reliable climatologies or actual aerosol data. Biomass-burning aerosols also need to be considered in savanna and forest regions. On a monthly timescale, however, the cloud-filtering procedure tends to select days with the lowest aerosol burden, reducing the effects of uncertainties on aerosol optical thickness in surface albedo estimates. In any case, even though the reliability of surface radiation data over the African continent may be questioned (Charlock 1996, personal communication), the systematic biases in the satellite estimates suggest that more effort is needed to account properly for the aerosol effects.

The use of thick clouds as constant reflectance targets to calibrate the Meteosat solar band (ISCCP procedure), may not adequately compensate for all changes due to sensor degradation. Large interannual variability in TOA reflectance was detected over a stable target such as the Libyan Desert, pointing to calibration errors and making it necessary to adjust the calibration coefficients.

Previous climatologies of downward surface solar irradiance and albedo have been obtained based on ISCCP C1 or ERBE data at about 2.5° of spatial resolution. This resolution may not be adequate to describe spatial variability in the ITCZ or regions of high vegetation gradient. In Fig. 8, mean surface albedo and downward solar irradiance at 30-km and 280-km resolutions are

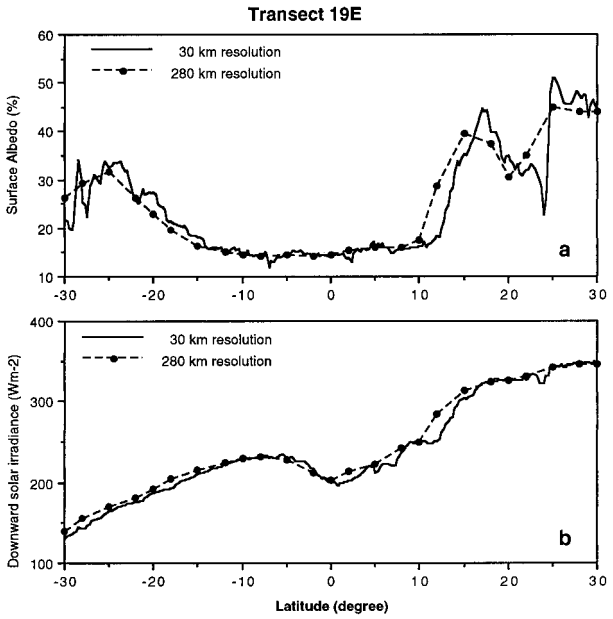

FIG. 8. Latitudinal transect of (a) mean surface albedo and (b) mean downward surface solar irradiance at 19°E for Jul 1983–88. Solid line denotes values obtained at 30-km resolution and dashed denotes line values at 280-km resolution.

compared along a latitudinal transect at 19°E for July 1983–88. The 280-km resolution data are degraded from the 30-km resolution data. For surface albedo (Fig. 8a), large differences are obtained in the savanna and semiarid regions, and may reach 100% in magnitude. In the Saharan region, the high-resolution data allow detection of the Tibesti Plateau's low albedo (0.2). For downward solar irradiance (Fig. 8b), noticeable differences are apparent between 0° and 15°N, a region that includes the ITCZ. Without the higher spatial resolution, important processes such as desertification in the Sahelian regions may not be detected or described properly.

Despite the limitations in the model and the uncertainties in the input variables, it can be argued that the proposed methodology is sufficiently accurate to describe spatial and seasonal changes in downward surface solar irradiance and albedo of the African continent, as well as interannual variability. The estimates compare generally well with those of other satellite algorithms, except Bishop's; they also agree to within 12% of ground-based measurements. Figure 8 further suggests that major spatial variability is described adequately. Although not shown here, seasonal variations of surface albedo appear to be well correlated and consistent with those of surface properties described by microwave data. These points, and the relationship between surface albedo and vegetation cover and soils, are explored in Part II of this series (Ba et al. 2001).

Acknowledgments. We wish to thank Mr. J. Kim of The Florida State University for programming support, and Dr. D. Tarpley at NOAA/NESDIS, Camp Springs, Maryland, for his critical reading of the manuscript. The SRB data (Darnell, Pinker, and Staylor estimates) used in the comparison are available at NASA Langley Research Center Distributed Active Archive Center. Bishop and Rossow estimates were provided by Dr. J. Bishop of Lamont–Doherty Geological Observatory, Columbia University, Palisades, New York. This work was sponsored by the NASA TRMM project under Grant NAG5-1587. Dr. Robert Frouin was supported by NASA under Grant NAGW-2727, and by the California Space Institute.

REFERENCES

Arino, O., G. Dedieu, and P. Y. Deschamps, 1991: Accuracy of satellite land surface reflectance determination. *J. Appl. Meteor.*, **30,** 960–972.

——, ——, and ——, 1992: Determination of land surface spectral reflectances using METEOSAT and NOAA/AVHRR shortwave channel data. *Int. J. Remote Sens.*, **13,** 2263–2287.

Ba, M. B., P. Y. Deschamps, and R. Frouin, 1995: Error reduction in NOAA satellite monitoring of the land surface vegetation during FIFE. *J. Geophys. Res.*, **100,** 25 537–25 548.

——, S. E. Nicholson, and R. Frouin, 2001: Satellite-derived surface radiation budget over the African continent. Part II: Climatologies of the various components. *J. Climate,* **14,** 60–76.

ben Mohamed, A., and J. P. Frangi, 1983: Humidity and turbidity parameters in Sahel: A case study for Niamey (Niger). *J. Climate Appl. Meteor.*, **22,** 1820–1823.

——, and ——, 1986: Results from ground-based monitoring of spectral aerosol optical thickness and horizontal extinction: Some characteristics of dusty Sahelian atmospheres. *J. Climate Appl. Meteor.*, **25,** 1807–1815.

——, ——, J. Fontan, and A. Druilhet, 1992: Spatial and temporal variations of atmospheric turbidity and related parameters in Niger. *J. Appl. Meteor.*, **31,** 1286–1294.

Bishop, J. K. B., and W. B. Rossow, 1991: Spatial and temporal variability of global surface solar irradiance. *J. Geophys. Res.*, **96,** 16 839–16 858.

Bréon, F. M., R. Frouin, and C. Gautier, 1994: Global shortwave energy budget at the earth's surface from ERBE observations. *J. Climate,* **7,** 309–324.

Brest, C. L., and W. B. Rossow, 1992: Radiometric calibration and monitoring of NOAA/AVHRR data for ISCCP. *Int. J. Remote Sens.*, **13,** 235–273.

——, ——, and M. D. Roiter, 1997: Update of radiance calibrations for ISCCP. *J. Atmos. Oceanic Technol.*, **14,** 1091–1109.

Cerf, A., 1980: Atmospheric turbidity over West Africa. *Contrib. Atmos. Phys.*, **53,** 414–428.

Charney, J. G., 1975: Dynamics of deserts and droughts in the Sahel. *Quart. J. Roy. Meteor. Soc.*, **101,** 193–202.

Courel, M. F., R. S. Kandel, and S. I. Rasool, 1984: Surface albedo and the Sahel drought. *Nature,* **307,** 528–531.

d'Almeida, G. A., 1986: A model for Saharan dust transport. *J. Climate Appl. Meteor.*, **25,** 903–916.

——, 1987: On the variability of desert aerosol radiative characteristics. *J. Geophys. Res.*, **92,** 3017–3026.

Darnell, W. L., W. F. Staylor, S. K. Gupta, and F. M. Denn, 1988: Estimation of surface insolation using sun-synchronous satellite data. *J. Climate,* **1,** 820–835.

——, ——, ——, N. A. Ritchey, and A. C. Wilber, 1992: Seasonal variation of surface radiation budget derived from International Satellite Cloud Climatology Project C1 data. *J. Geophys. Res.*, **97,** 15 741–15 760.

Dedieu, G., P. Y. Deschamps, and Y. H. Kerr, 1987a: Satellite estimation of solar irradiance at the surface of the earth and of

surface albedo using a physical model applied to METEOSAT data. *J. Climate Appl. Meteor.*, **26,** 79–87.

——, ——, ——, and P. Raberanto, 1987b: A global survey of surface climate parameters from satellite observations: Preliminary results over Africa. *Adv. Space Res.*, **11,** 129–137.

Deering, D. W., 1989: Field measurements of bidirectional reflectance. *Theory and Applications of Optical Remote Sensing*, G. Asrar, Ed., John Wiley and Sons, 14–65.

Desormeaux, Y., W. B. Rossow, C. L. Brest, and G. G. Campbell, 1993: Normalization and calibration of geostationary satellite radiances for the International Satellite Cloud Climatology Project. *J. Atmos. Oceanic Technol.*, **10,** 304–325.

Dickinson, R. E., 1983: Land surface processes and climate-surface albedos and energy balance. *Advances in Geophysics*, Vol. 25, Academic Press, 305–353.

DiPasquale, R. C., P. A. Quigley, C. H. Whitlock, A. Tsvetkov, and S. Wilcox, 1996: 1986 daily daylight cloud fraction, shortwave surface radiation, and transmittance for 502 sites. NASA Tech. Memo. 110245, 359 pp. [Available from NASA Langley Research Center, Hampton, VA 23681-0001.]

Faizoun, C. A., A. Podaire, and G. Dedieu, 1994: Monitoring of Sahelian aerosol and atmospheric water vapor content characteristics from sun photometer measurements. *J. Appl. Meteor.*, **33,** 1291–1303.

Fouquard, Y., B. Bonnell, G. Brogniez, J. C. Buriez, L. Smith, J. J. Morcrette, and A. Cerf, 1987a: Observations of Saharan aerosols: Results of ECLATS field experiment. Part II: Broadband radiative characteristics of the aerosols and vertical radiative flux divergence. *J. Climate Appl. Meteor.*, **26,** 38–52.

——, ——, M. Chaoui Roquai, and R. Santer, 1987b: Observations of Saharan aerosols: Results of ECLATS field experiment. Part I: Optical thicknesses and aerosol size distributions. *J. Climate Appl. Meteor.*, **26,** 28–37.

Frouin, R., and B. Chertock, 1992: A technique for global monitoring of net solar irradiance at the ocean surface. Part I: Model. *J. Appl. Meteor.*, **31,** 1056–1066.

Gautier, C., G. Diak, and S. Masse, 1980: A simple physical model to estimate incident solar radiation at the surface from GOES satellite data. *J. Appl. Meteor.*, **19,** 1005–1012.

Gupta, S. K., 1989: A parameterization for longwave surface radiation from sun-synchronous satellite data. *J. Climate*, **2,** 305–320.

Gutman, G. G., 1992: Anisotropy of visible and near-IR reflectances over land as observed from NOAA AVHRR. *IRS '92: Current Problems in Atmospheric Radiation*, S. Keevallik and O. Käner, Eds., A. Deepak Publishing, 436–439.

Holben, B. N., T. F. Eck, and R. S. Fraser, 1991: Temporal and spatial variability of aerosol optical depth in the Sahel region in relationship to vegetation remote sensing. *Int. J. Remote Sens.*, **12,** 1147–1164.

Kimes, D. S., 1983: Dynamics of directional reflectance factor distribution for vegetation canopies. *Appl. Opt.*, **22,** 1364–1372.

Kriebel, K. T., 1978: Measured spectral bidirectional reflection properties of four vegetated surfaces. *Appl. Opt.*, **17,** 253–259.

Legrand, M., J. J. Bertrand, and M. Desbois, 1985: Dust clouds over West Africa: A characterization by satellite data. *Ann. Geophys.*, **3,** 777–784.

——, M. Desbois, and K. Vovor, 1988: Satellite detection of Saharan dust: Optimized imaging during nighttime. *J. Climate*, **1,** 256–265.

London, J., R. D. Bojkov, S. Oltmans, and J. I. Kelley, 1976: Atlas of the global distribution of total ozone July 1957–June 1967. National Center for Atmospheric Research Tech. Note 113+STR, University Corporation for Atmospheric Research, Boulder, CO, 276 pp.

Matthews, E., 1983: Global vegetation and land-use: New high-resolution data bases for climate studies. *J. Climate Appl. Meteor.*, **22,** 474–487.

Moulin, C., C. E. Lambert, F. Guillard, J. Poitou, F. Cabot, G. Dedieu, and F. Dulac, 1994: Calibration of long time series of METEOSAT visible images. *Proc. 10th METEOSAT Scientific Users' Conf.*, Cascais, Portugal, EUMETSAT, 351–358.

N'Tchayi, G. M., J. Bertrand, and S. E. Nicholson, 1997: The diurnal and seasonal cycles of wind-borne dust over Africa north of the equator. *J. Appl. Meteor.*, **36,** 868–882.

Pinker, R. T., and J. A. Ewing, 1985: Modelling surface solar radiation: Model formulation and validation. *J. Climate Appl. Meteor.*, **24,** 389–401.

——, and I. Laszlo, 1992: Modeling surface solar irradiance for satellite applications on a global scale. *J. Appl. Meteor.*, **31,** 194–211.

——, G. Idemudia, and T. O. Aro, 1994: Characteristic aerosol optical depths during the Harmattan season in sub-Saharan Africa. *Geophys. Res. Lett.*, **21,** 685–688.

Pinty, B., and G. Szejwach, 1985: A new technique for inferring surface albedo from satellite observations. *J. Climate Appl. Meteor.*, **24,** 741–750.

——, and D. Ramond, 1987: A method for estimate of broadband directional surface albedo from a geostationary satellite. *J. Climate Appl. Meteor.*, **26,** 1709–1722.

——, and D. Tanré, 1987: The relationship between incident and double-way transmittances: An application for the estimate of surface albedo from satellites over the African Sahel. *J. Climate Appl. Meteor.*, **26,** 892–896.

——, G. Szejwach, and J. Stum, 1985: Surface albedo over the Sahel from METEOSAT radiances. *J. Climate Appl. Meteor.*, **24,** 108–113.

Rahman, H., and G. Dedieu, 1994: SMAC: A simplified method for the atmospheric correction of satellite measurements in the solar spectrum. *Int. J. Remote Sens.*, **15,** 123–143.

Ramanathan, V., B. R. Barkstrom, and E. F. Harrison, 1989: Climate and the earth radiation budget. *Phys. Today*, **42,** 22–32.

Raschke, E., A. Gratzki, and M. Rieland, 1987: Estimates of global radiation at the ground from the reduced data sets of the International Satellite Cloud Climatology Project. *J. Climatol.*, **7,** 205–213.

Rossow, W. B., and Y.-C. Zhang, 1995: Calculation of surface and top-of-atmosphere radiation fluxes from physical quantities based on ISCCP datasets. Part II: Validation and first results. *J. Geophys. Res.*, **100,** 1167–1197.

——, Y. Desormeaux, C. L. Brest, and A. Walker, 1992: International Satellite Cloud Climatology Project (ISCCP) radiance calibration report. WMO/TD-520, WCRP-77, World Meteorological Organization, Geneva, Switzerland, 104 pp.

Tanré, D., C. Deroo, P. Duhaut, M. Herman, J. J. Morcrette, J. Perbos, and P. Y. Deschamps, 1990: Description of computer code to simulate the satellite signal in the solar spectrum: The 5S code. *Int. J. Remote Sens.*, **11,** 659–668.

Tarpley, J. D., 1979: Estimating incident solar radiation at the surface from geostationary satellite data. *J. Appl. Meteor.*, **18,** 1172–1181.

Tuller, S. E., 1968: World distribution of mean monthly and annual precipitable water. *Mon. Wea. Rev.*, **96,** 785–797.

Whitlock, C. H., and Coauthors, 1990: Comparison of surface radiation budget satellite algorithms for downwelled shortwave irradiance with Wisconsin FIRE/SRB surface truth data. Preprints, *Seventh Conf. on Atmospheric Radiation*, San Francisco, CA, Amer. Meteor. Soc., 237–242.

——, and Coauthors, 1995: First global WCRP shortwave surface radiation budget dataset. *Bull. Amer. Meteor. Soc.*, **76,** 905–922.

World Climate Research Programme, 1983: Report of the experts meeting on aerosols and their climatic effects. WCP Rep. 55, WMO, 107 pp.

Yamamoto, G., 1962: Direct absorption of solar radiation by atmospheric water vapor, carbon dioxide and molecular oxygen. *J. Atmos. Sci.*, **19,** 182–188.

Zhang, Y.-C., W. B. Rossow, and A. A. Lacis, 1995: Calculation of surface and top-of-atmosphere radiation fluxes from physical quantities based on ISCCP datasets. Part I: Method and sensitivity to input data uncertainties. *J. Geophys. Res.*, **100,** 1149–1165.